FR 820 3133

institut de physique nucléaire
LABORATOIRE ASSOCIÉ A L'IN2P3

IPNO-DRE-82-09

DECAYS OF $^{185m+g}$Hg : LOW-SPIN LEVELS OF ^{185}Au AS A TEST OF NUCLEAR MODELS

C. Bourgeois*, P. Kilcher, B. Roussière,
J. Sauvage-Letessier,
Institut de Physique Nucléaire, 91406 Orsay, France

M.G. Porquet
Centre de Spectrométrie Nucléaire et de Spectrométrie de Masse, 91406 Orsay, France

and

The ISOCELE Collaboration.

UNIVERSITÉ PARIS-SUD

DECAYS OF $^{185m+g}Hg$: LOW-SPIN LEVELS OF ^{185}Au AS A TEST OF NUCLEAR MODELS.

C. BOURGEOIS*, P. KILCHER, B. ROUSSIERE, J. SAUVAGE-LETESSIER
Institut de Physique Nucléaire, 91406 ORSAY, FRANCE
M.G. PORQUET
Centre de Spectrométrie Nucléaire et de Spectrométrie de Masse, 91406 ORSAY, FRANCE
and
The ISOCELE Collaboration.

Abstract : The decay of $^{185m+g}Hg$ has been studied on-line with mass-separated sources from the ISOCELE facility. Precise conversion-electron measurements were performed with a 180° spectrograph. The 13/2+ isomeric-state of ^{185}Hg ($T_{1/2}$ = 28 ± 5 s) was located with respect to the 1/2- ground-state ($T_{1/2}$ = 55 ± 10 s). A level scheme of ^{185}Au has been established. Two abnormally converted M1 transitions de-excite a state located at 330.2 keV. Excited states of ^{185}Au have been discussed in the framework of a "quasi-particle + axial rotor" approach, quasi-particle states being issued from Hartree-Fock plus BCS calculations using the SIII Skyrme force. Most of the low-spin negative-parity levels have been identified as $h_{9/2}$ + $f_{5/2}$ or $p_{3/2}$ + $f_{7/2}$ mixed states. The $h_{11/2}$ system has also been discussed using a model of a single-j quasi-particle coupled to a triaxial rotor.

E | RADIOACTIVITY ^{185}Hg (from Au(p,xn)Hg, on-line mass-separated) ; measured E_γ, I_γ, E_{ce}, I_{ce}, γ-γ coin, γ-X coin. Deduced ^{185m}Hg IT decay branching, ^{185}Hg deduced levels, ^{185}Au deduced levels, J, Π, ICC, multipolarities. Ge(HP), Ge(Li), Si(Li), magnetic spectrograph.

* and Université PARIS VII

1 - INTRODUCTION

The odd-A neutron-deficient Au nuclei lie in a very complex transitional region where several states, corresponding to different nuclear deformations, occur within about the same excitation energy. Extensive experimental works (refs[1-13]) and theoretical studies (refs [14-21]) have been already carried out in this area, especially on $_{77}$Ir, $_{79}$Au and $_{81}$Tl isotopes. This considerable amount of informations bring us to understand in a more accurate way some specific features occurring in this region. When the neutron number N decreases, the nuclear deformation is expected to increase and eventually to become maximum for N = 104, 106. Consequently ^{185}Au should exhibit a rather large deformation compared to the heavier odd-A Au isotopes and new characteristic levels should appear. Therefore it was very interesting to extend the systematic study of high-spin and low-spin states of the Au-nuclei down to A = 185 in order to improve our comprehension of the observed phenomena.

In a previous work, the ^{185}Au high-spin states have been investigated by means of (HI,xn) reactions and a level scheme has been already established [11]. The $_{79}$Au proton Fermi level lying above the $h_{11/2}$ proton shell and below the $h_{9/2}$ and $i_{13/2}$ proton shells, the three families of states observed in ^{185}Au have been interpreted as collective excitations originating from the coupling of the $\pi h_{9/2}$, $\pi i_{13/2}$ particle-states and $\pi h_{11/2}$ hole-state to the core according to the rotation-alignment coupling scheme [22]. In the framework of this model, the level sequence of the collective bands give direct information on the shape of the nucleus. The observation of three $\Delta I=2$ decoupled bands in ^{185}Au thus infers the coexistence of two different shapes in this nucleus : the band built on an 11/2- state from h11/2 corresponds to an oblate shape while the others, built on a 9/2- and a 13/2+ state from $h_{9/2}$ and $i_{13/2}$ respectively, correspond to a prolate shape. Oblate $h_{11/2}$ and prolate $h_{9/2}$ systems also coexist in ^{187}Au [6] and ^{189}Au [9].

From (HI,xn) reaction measurements only, the 11/2-, 9/2- and 13/2+ band-head states of ^{185}Au have not been located with respect to the 5/2 [23] ground-state. Additional investigations using ^{185}Hg radioactive decay were required to obtain a comprehensive low-energy level scheme of ^{185}Au.

We present here the results concerning the ^{185}Au levels populated by the $\beta+/EC$ decay of ^{185}Hg. Mercury isotopes were produced by Au(p,xn)Hg reactions then mass-separated using the ISOCELE II facility at Orsay[24]. ^{185}Hg nuclei being produced in the 13/2+ [25] isomeric state and in the 1/2- [26] ground-state as well, ^{185}Au states with spin values as high as 17/2 are populated in the decay of $^{185m+g}Hg$. In this way, we have been able to locate exactly the 9/2-, 11/2- and 13/2+ band-head states already observed from (HI,xn) reactions. Furthermore, the great number of low-spin states established in ^{185}Au do provide a stringent test of the theoretical approaches, high spin yrast levels being less sensitive to the parameters of various nuclear models. Some preliminary results have already been published in several conference proceedings[27].

2 - EXPERIMENTAL PROCEDURES

2.1 - Radioactive isotope production

The excited states of ^{185}Au were studied from the $\beta+/EC$ decay of ^{185}Hg. In order to produce mercury, a target of about 1 cm^3 molten gold was continuously irradiated by a 200 MeV proton beam from the Orsay Synchrocyclotron (proton beam intensity $I_p = 2.5$ µA). Mercury isotopes produced by Au(p,xn)Hg reactions were evaporated from the gold target placed inside the ion source of the ISOCELE II isotope separator [24]. The extracted Hg ions were mass-separated in a magnetic field and then collected on a mylar/aluminum tape. The obtained radioactive sources were carried from the collecting point to the counting point using a fast mechanical tape-transport system.

2.2 - Gamma-ray spectroscopy

Singles gamma-rays over the energy range from 20 keV to 500 keV were measured with a planar Ge(HP) X-ray detector (resolution 0.6 keV FWHM at 122 keV). Higher efficiency coaxial Ge(HP) and Ge(Li) detectors were used to study γ-rays of higher energy (up to 2 MeV). An example of the γ-singles spectra from the decay of $^{185m+g}Hg$ is presented in fig.1. X-γ-t and γ-γ-t coincidence events were simultaneously recorded in event-by-event mode on magnetic tape. The experimental data were treated on the Orsay IBM 360-370 computer. The γ-singles spectra have been analysed using the SAMPO curve-fitting code and the coincidence events treated in order to get prompt and delayed coincidence bidimensional matrices. The background-corrected coincidence spectra, shown as examples in fig.2, were constructed by setting gates on the time spectrum and on selected peaks of interest.

2.3 - Electron spectroscopy

The singles electron spectra were first measured using a cooled 3 mm thick Si(Li) detector (resolution 3 keV FWHM at 624 keV). The occurrence of numerous transitions with energy lower than 500 keV did not allow us to determine, to a satisfactory precision, the intensities of the electron lines. To improve the electron measurements, the low-energy spectrum has been recorded on the photographic plate of a 0.2% resolution semi-circular magnetic spectrograph working on-line with the mass-separator. Magnetic inductions of $4.2\ 10^{-3}$, $5\ 10^{-3}$, 10^{-2} and $1.3\ 10^{-2}$ Tesla were used in order to cover an energy range from 10 keV to 430 keV. The photographic plates were analysed with a PDS microdensitometer at the C.D.S.I. Institut d'Optique (Orsay) [28]. The data were recorded on magnetic tapes and then treated with curve-fitting programs on the IBM 138-370 computer. Typical conversion-electron spectra are shown in fig. 3 and fig. 4.

2.4 - Determination of half-lives

Singles γ-rays and conversion-electron data were taken in multispectrum modes to obtain informations about half-lives. The conversion-electron spectra were measured with a cooled Si(Li) detector, a magnetic field being used in order to eliminate the β+ background and to prevent X- and γ-rays to reach the detector [29].

3 - EXPERIMENTAL RESULTS

3.1 - Half-life measurements

The decay half-lives of ^{185m}Hg and ^{185}Hg have been determined to be $T_{1/2}$ = 28 ± 5 sec and $T_{1/2}$ = 55 ± 10 sec respectively. The attribution of the shortest half-life to the ^{185m}Hg 13/2+ isomeric state is inferred from the result obtained on the multiscaling of the γ-rays corresponding to transitions between high-spin states (17/2 → 13/2, 13/2 → 9/2, 15/2 → 11/2, etc...) in ^{185}Au. Consequently the $T_{1/2}$= 55 ± 10 s half-life has been attributed to the ^{185g}Hg 1/2- ground-state. These results are in agreement with previously reported values [30].

3.2 - The level scheme of ^{185}Au

The energies and intensities of the γ-rays assigned to the $^{185m+g}Hg$ decay and the corresponding conversion-electron intensities are listed in table 1 together with the deduced transition multipolarities. The main coincident γ-rays are also indicated. From these results, a level scheme of ^{185}Au has been built (figs. 5 and 6). In making spin and parity assignments, we started out from firm assignments : the ^{185}Au 5/2 ground-state spin has been measured by ABMR method [23] and the high-spin states (9/2 < I < 17/2) populated in the decay of ^{185m}Hg have already been established by (HI,xnγ) measurements [11]. The spin and parity assignments for previously unknown levels are derived from the multipolarities of the transitions. The transitions in ^{185}Au can be classified into two groups when connecting either high-spin states or low-spin states, since levels with spin lower than 5/2 are mainly populated in the decay of ^{185g}Hg ($T_{1/2}$= 55 sec) while those with spin higher than 9/2 are populated in the decay of ^{185m}Hg ($T_{1/2}$= 28 sec) : this has been used in order to discriminate between possible spin values of some states. Moreover log ft values for β+/EC decay to some low-spin individual levels were deduced from a Q_{EC} of 6.59 MeV [31], the ^{185g}Hg decay scheme and the tables of Gove and Martin [32].

The 5/2 ground-state of ^{185}Au can be interpreted as the 5/2- rotational state of the $h_{9/2}$ system and, from systematic study of the heavier odd-A Au isotopes, the 9/2- bandhead is expected to be very close to the ground-state. The existence of the 107 keV doublet added to the γ-γ coincidence results (gate set on the 193.7 keV γ-ray line) have allowed us to locate the 9/2- level at 8.9 keV with respect to the 5/2- ground-state. The lifetime of the 8.9 keV state has been measured [33] which confirms the existence of the 9/2- → 5/2- transition.

The γ-γ coincidence results involve all the main transitions with energy higher than 30 keV. The conversion electron spectra have revealed two additional low-energy transitions of 17.2 and 23.6 keV. The 17.2 keV (M1 + E2) transition has been assigned as the transition de-exciting a 3/2- state to the 5/2- ground-state : the 5/2 and 7/2 spin values have been eliminated for this 17.2 keV state, the calculated log ft value being lower than the log ft limit [34)] of the second-forbidden non-unique transition β-decay. Noting that (17.4 ± 0.2) keV is the energy difference between the 210.4 and the 193.0 keV γ-lines, numerous negative parity states established by the γ-γ coincidence results have been connected to the 17.2 keV 3/2- state (fig.5). The M2 character of the 23.6 keV transition supports its location between a 1/2+ state (expected from systematics) and the 5/2- ground-state : one has to notice that this transition is the only connection between the low-spin positive-parity state system and the negative-parity state system. The above mentioned positive-parity levels are populated by the decay of the 1/2- ground-state of ^{185}Hg ($T_{1/2}$= 55 s) and thus, only spins lower than or equal to 5/2 are expected.

The 3/2- spin and parity have been unambiguously attributed to the 190.1 keV state inferred from the log ft value for the β+/EC decay to this level and from the 190.1 keV transition multipolarity.

The 330.2 keV level de-excites towards the 9/2- (8.9 keV) and 5/2- ground-state via the 321.4 keV and the 330.2 keV transitions respectively : in such a way the large conversion coefficients of these two transitions (table 1) cannot be due to the existence of an E0 component, but are believed to correspond to abnormally converted M1 transitions (arising from dynamic penetration effects of the electronic wave-function inside the nucleus). Consequently the spin and parity values 7/2- can be attribuated to the 330.2 keV state.

3.3 - The IT decay of ^{185m}Hg

The detailed analysis of the low-energy electron spectrum (fig.3) has clearly established the existence of two transitions occurring in ^{185}Hg, namely a (M1 + E2) 26.1 keV and an E3 65.3 keV transitions (table 2). Due to the high-precision e^- energy measurements with the magnetic spectrograph, the transitions converted in ^{185}Hg have been unambiguously distinguished from those converted in ^{185}Au using the energy differences between the various L, M atomic subshells in gold and mercury.

The multiscaling of the 65.3 L electron lines leads to the half-life $T_{1/2} = 30 \pm 4$ sec which is, within the error limits, the half-life of the 13/2+ isomeric state of ^{185}Hg : therefore, ^{185m}Hg decays partly by isomeric transition and partly by β+/EC mode. The total intensities of the 26.1 keV and 65.3 keV transitions are similar which suggests to order them in cascade. With the help of the decay scheme of ^{185m}Hg to ^{185}Au, the total isomeric transition probability is deduced to be (54 ± 10)%. This result is in fair agreement with previous measurements [30,35] but the isomeric transition was hitherto unobserved.

4 - DISCUSSION

4.1 - Levels in ^{185}Hg

The occurrence of a 65.3 keV E3 isomeric transition in ^{185}Hg suggests a 13/2+ → 7/2- transition. The hindrance factor of such an E3 transition, calculated relative to the theoretical single-particle Weisskopf estimate, using the theoretical γ transition probability P_γ (theo) = 35 A^2 E_γ^7 given in ref. [31], is F_W = 550 ± 70. One has to remember that the 1/2-[521] ground-state of ^{185}Hg corresponds to a large prolate deformation of the nucleus [26], contrary to the heavier odd-A quasi-spherical Hg isotopes : a new set of low-energy levels is then expected to occur in ^{185}Hg, as for instance the 7/2-[514] state. The de-excitation of such a 7/2- state directly towards the 1/2- ground state would imply a M3 transition : instead of that, we detect a (M1 + E2) 26.1 keV transition which can take place either between the 7/2- level and a 5/2- level or between a 3/2- level and the 1/2- ground-state. The energy of the unobserved remaining E2 transition in the cascade 7/2 → 5/2 (→) 1/2 or 7/2 (→) 3/2 → 1/2 should be less than 15 keV. From the systematics of the low-spin states through the N = 105 isotones [36], the presence of a 5/2- state at so low energy in ^{185}Hg is difficult to understand and for this reason, we are in favor of the level scheme presented in fig.7 with a 3/2- level at 26.1 keV. This level could be considered as the 3/2 1/2-[521] state.

4.2 - Levels in ^{185}Au

The energy levels of the odd-A transitional nuclei lying in the A = 183-193 region are rather well described by the "quasi-particle + rotating core" coupling scheme. Especially the "quasi-particle + triaxial rotor" model of J. Meyer-ter-Vehn [37] has been widely used with great success to explain the high-spin levels related to high-j unique parity orbitals, such as $h_{11/2}$ and $i_{13/2}$. However, many features involving low-j and/or mixed-j sub-shells cannot be understood without a more general treatment. In such a way, M. Meyer et al [38] have developped a "quasi-particle + axial rotor" coupling treatment taking into account all the quasi-particle states lying near the Fermi level. In that approach, the single-particle wave-functions are extracted from self-consistent calculations for the core using Hartree-Fock (HF)-plus-BCS treatment with the SIII Skyrme effective force. The static deformation of the odd nucleus is assumed to be the same as the core corresponding to the minimum in the deformation energy curve. The expansion of the wave-functions onto states having a good core angular momentum R allows the inclusion of experimental moment of inertia $\mathcal{J}(R)$ (extracted from the experimental core energies) into the Hamiltonian. The Coriolis interaction between the quasi-particle and the rotor is exactly solved. One can remark that the self-consistent effects of the odd-particle on the core properties are neglected and that this model describes the A-1 and the A+1 nucleus for a given even-even core A, depending upon the position of the HF level (corresponding to the considered quasi-particle state) with respect to the Fermi level. This model has already been applied with success to transitional nuclei ($|\beta_2| \sim 0.15$), to deformed nuclei ($\beta_2 \sim 0.3$) and even to fission isomers ($\beta_2 \sim 0.6$) [38,39].

The results of (HI,xnγ) experiments gave firm evidence of shape coexistence in ^{185}Au : prolate shape for the 5/2- ground- and 13/2+ (860.1 keV)- state and oblate shape for the 11/2- (220.1 keV)-state. Therefore, the theoretical calculations of levels in ^{185}Au have been performed from ^{184}Pt and ^{186}Hg cores, for the prolate and oblate minima of the potential energy surfaces [20], and taking into account all the HF states located in a 10 MeV band around the Fermi level.

We have, in a first step, focused our attention to the negative-parity states related to the 5/2- prolate ground-state. Thus the quasi-particle states used in the calculation have been extracted from the HF prolate equilibrium solution for ^{184}Pt (β_2= 0.27) and ^{186}Hg (β_2= 0.28), and the $\mathcal{J}$(R) values used in the core Hamiltonians have been extracted from the experimental energies of the ground-state rotational band of ^{184}Pt [31] and of the deformed rotational band of ^{186}Hg [40]. The ^{185}Au experimental levels and the theoretical states calculated from the two cores are presented in fig.8 : all the states with energy lower than 1 MeV (relative to the 5/2- ground-state) are shown. The calculated states can be classified into two families, the first one originating from the coupling of the ($h_{9/2}$ + $f_{5/2}$) quasi-particle states to the core, the second one mainly from the coupling of the ($p_{3/2}$ + $f_{7/2}$) quasi-particle states to the core. The wave-functions of the low-energy negative-parity states (up to 300 keV) are presented in table 3 in terms of the square of their overlap with the spherical harmonic oscillator basis nlj : none of these states exhibit a unique-j configuration and that is the case even for the levels previously labelled as pure $h_{9/2}$ states such as the 9/2- (8.9 keV) level.

The comparison between experiment and theory presented in fig.8 allows the identification of most of the experimental levels. Particularly the levels at 190.1 keV (3/2-), 267.5 keV (1/2-, 3/2-, 5/2-), 288.7 keV (3/2-, 5/2-, 7/2-), 559.4 keV (5/2-) and 926.3 keV (9/2-) can be respectively assigned to be the 3/2-, 1/2-, 7/2-, 5/2- and 9/2- states which come from the coupling of the ($p_{3/2}$ + $f_{7/2}$) quasi-particle states to the core. One has to remark that the calculation using the ^{186}Hg core gives a better agreement between the experimental and theoretical results. The system of experimental levels related to the 5/2- ground-state can be separated into rotational bands built on different HF states (fig.9) inferred from the theoretical results using the deformed ^{186}Hg core.

We have also displayed in fig. 9 the experimental levels that our calculations cannot explain. Among them, two levels located at 330.2 and 535.4 keV are particularly interesting because the 321.4, 330.2 and the 205.2 keV transitions de-exciting them exhibit large conversion coefficients. The Very Converted Transitions (VCT) of 321.4 and 330.2 keV are abnormally converted M1 transitions (cf § 3.2). VCT have already been observed in some odd-A nuclei close to ^{185}Au : ^{187}Pt [41), ^{187}Au [42)] $^{193,195,197}Hg$ [43)]. Most of these VCT have been assigned as E0 + M1 (+E2) transitions. Complementary measurements should be done in order to check the occurrence of large E0 components in these VCT.

The energy levels related to the 11/2- (220.1 keV) state have been analyzed in the framework of the "HF quasi-particle + axial rotor" treatment, the qp states being calculated in the HF field of the oblate equilibrium solution for ^{186}Hg (β_2 = -0.19). A quite poor agreement is found between the experimental and theoretical levels, especially no explanation is found for the bunching of states around the 15/2- (682.3 keV) level. But a clear indication of quasi-pure ($\sim$ 90%) $h_{11/2}$ configuration is found for the 11/2- (220.1 keV) state. In that respect, the "quasi-particle + triaxial rotor" of J. Meyer-ter-Vehn [37)] can be used in order to test the influence of the asymmetry parameter γ on the level sequence. In figure 10, the systematics of experimental levels and corresponding theoretical states coming from the h11/2 subshell are shown for the odd-A gold isotopes from A = 185 to A = 193. The energy of the 9/2- and 13/2- states is closely related to the asymmetry parameter γ and the best agreement between the experimental and theoretical results is obtained with γ = 34° in $^{187,189,191,193}Au$ and with γ = 30° in ^{185}Au. In an other hand, the inversion of the 9/2- and 13/2- states between ^{189}Au and ^{187}Au is related to the position of the Fermi level λ_F inside the $h_{11/2}$ subshell.

Firm spin assignment for the low-lying positive-parity levels is somewhat uneasy except for the 1/2+ (23.6 keV) state. Comparison with heavier Au-isotopes positive-parity systems does not shed any light on this, particularly the de-excitation modes of the first excited states of ^{185}Au are found quite different. In spite of that, the experimental levels are compared (fig.11) with the theoretical states obtained from the "HF qp + axial rotor" treatment, the quasi-particle states being calculated in the HF field of the oblate (β_2 = -0.19) and prolate (β_2 = 0.28) equilibrium solutions for ^{186}Hg. It seems that a better agreement is found when assuming an oblate-shaped core. As demonstrated before for the oblate $h_{11/2}$ system, the γ parameter could also play an important role in the low-spin positive-parity pattern. The mixing of the wave functions is very important as foreseeable, thus the "qp + triaxial rotor" model of J. Meyer-ter-Vehn cannot be used.

In an extended version [18] of the "particle + asymmetric rotor" model (Hecht-Satchler) where the odd proton occupies different orbitals of the deformed (ε,γ) Nilsson potential, the low-lying positive parity levels of $^{193-199}$Au and $^{187-193}$Ir nuclei have been rather well explained by use of $\varepsilon = 0.17$, $\gamma = 27°$ [18] and $\varepsilon = 0.20$, $\gamma = 25°$ [44] deformation parameter values respectively.

Recently another approach has been used by Wood [45] for ^{193}Au where the positive-parity states are discussed in terms of a dynamical super-symmetry generated by L = 0,2 bosons with O(6) symmetry and a fermion with j = 3/2 ($d_{3/2}$) : it is pointed out that the $1/2^+_1$ is a member of the multiplet built on the j = 3/2 level ($d_{3/2}$). Unfortunately the B(M1) value for the $1/2^+_1 \rightarrow 3/2^+_1$ transition which has been calculated, not in ^{193}Au but in the ^{191}Ir isotone [46], exhibits a large discrepancy with the experimental reduced transition probability.

Finally, no definitive conclusion concerning the low-lying positive-parity levels of ^{185}Au can be drawn, due to the paucity of excited states populated by the decay of ^{185}Hg. In particular the presence at 860.1 keV of a 13/2+ yrast state from the $i_{13/2}$ subshell hinders the observation of higher-spin (> 5/2) rotational states built on the $3/2^+_1$ and $1/2^+_1$ levels.

5 - CONCLUSION

The study of heavy nuclei by radioactive decay in regions far from beta-stability requires high-precision detection of γ-rays and conversion-electrons. In the investigation of the decay of $^{185m+g}$Hg, a 0.2% resolution electron spectrograph working on-line to the ISOCELE isotope-separator has been used : in that way, it has been possible to measure the transition energy with good accuracy and to determine the transition multipolarities. Two transitions have been assigned to ^{185}Hg and a de-excitation scheme of ^{185m}Hg could be proposed with the 13/2+ isomeric-state at 99 ± 8 keV above the 1/2- ground-state.

Numerous low-spin levels have been established in ^{185}Au. Most of the low-spin negative-parity levels related to the 5/2- ground-state have been interpreted in terms of a "HF qp + axial rotor" coupling scheme. They have been classified into two families of states which are not due to pure high-j subshells but to $h_{9/2} + f_{5/2}$ and $p_{3/2} + f_{7/2}$ admixtures respectively. These states correspond to a well-deformed prolate nucleus. The occurrence of low-lying states originating from the $f_{7/2}$ and $p_{3/2}$ subshells supports the contention that β-deformation is larger in ^{185}Au than in the heavier odd-A Au isotopes.

In addition to previously reported results from (HI,xnγ) experiments, two levels related to the oblate $h_{11/2}$ system have been observed. Their interpretation needs to take into account the asymmetry γ of the nucleus. The states of the $h_{11/2}$ system are well reproduced with γ = 30°.

Moreover our experimental work has shown the existence of at least two abnormally converted M1 transition in ^{185}Au. This last result is not yet well understood.

We would like to thank the staff of the ISOCELE separator for technical assistance in particular in the course of the numerous delicate experiments using the β-spectrograph. We are indebted to the staff of the Orsay Synchrocyclotron for their cooperation. We thank Dr. P. Paris who allowed us to use his "Si(Li) electron detector + magnetic selector" system. We are also grateful to Pr. Ph. Quentin and Dr. M. Meyer for their fruitful collaboration and Dr. J. Meyer-ter-Vehn for providing us with copy of his program.

REFERENCES

1 - C. Schück, J. Genevey-Rivier, V. Berg, A. Knipper, W. Walter, C. Richard-Serre and A. Höglund,
Nucl. Phys. A325 (1979) 421.

2 - C. Sébille-Schück, M. Finger, R. Foucher, J.P. Husson, J. Jastrzebski, V. Berg and S.G. Malmskog,
Nucl. Phys. A212 (1973) 45.

3 - S. André, J. Boutet, J. Rivier, J. Tréherne, J. Jastrzebski, J. Lukasiak and Z. Sujkowski,
Nucl. Phys. A243 (1975) 229.

4 - P. Kemnitz, L. Funke, H. Sodan, E. Will and G. Winter,
Nucl. Phys. A245 (1975) 221.

5 - V. Berg, R. Foucher and A. Höglund,
Nucl. Phys. A244 (1975) 462.

6 - M.A. Deleplanque et al.
J. de Phys. Lett. 36 (1975) 205 ;
- C. Bourgeois, P. Kilcher, J. Letessier, V. Berg and M.G. Desthuilliers,
Nucl. Phys. A295 (1978) 424.

7 - Y. Gono, R.M. Lieder, M. Müller-Veggian, A. Neskakis and C. Mayer-Böricke,
Nucl. Phys. A327 (1979) 269.

8 - Ch. Vieu, A. Péghaire and J.S. Dionisio,
Rev. Phys. Appl. 8 (1973) 231.

9 - M.A. Deleplanque, C. Gerschel, N. Perrin and V. Berg,
Nucl. Phys. A249 (1975) 366.

10 - E.F. Zganjar et al.
Phys. Lett. 58B (1975) 159.

11 - M.G. Desthuilliers, C. Bourgeois, P. Kilcher, J. Letessier, F. Beck T. Byrski and A. Knipper,
Nucl. Phys. A313 (1979) 221.

12 - J.O. Newton, F.S. Stephens and R.M. Diamond,
Nucl. Phys. A236 (1974) 225.

13 - A.G. Schmidt, R.L. Mlekodaj, E.L. Robinson, F.T. Avignone III, J. Lin, G.M. Gowdy, J.L. Wood and R.W. Fink,
Phys. Lett. 66B (1977) 133.

14 - A.L. Goodman,
Nucl. Phys. A287 (1977) 1.

15 - H. Toki and A. Faessler,
Nucl. Phys. A253 (1975) 231.

16 - J. Meyer-ter-Vehn,
Phys. Lett. 55B (1975) 273.

17 - F. Iachello,
Phys. Rev. Lett. 44 (1980) 772.

18 - Ch. Vieu, S.E. Larsson, G. Leander, I. Ragnarsson, W. de Wieclawik and J.S. Dionisio,
J. Phys. G : Nucl. Phys. 4 (1978) 531 and 1159.

19 - Y. Tanaka and R.K. Sheline,
Nucl. Phys. A276 (1977) 101.

20 - J. Sauvage-Letessier, P. Quentin and H. Flocard,
Nucl. Phys. A370 (1981) 231.

21 - R. Piepenbring,
Z. Phys. A297 (1980) 73.

22 - F.S. Stephens,
Rev. of Mod. Phys. 47 (1975) 43.

23 - C. Ekström, L. Robertsson, S. Ingleman, G. Wannberg and I. Ragnarsson,
Nucl. Phys. A348 (1980) 25.

24 - P. Paris et al.
Nucl. Inst. and Methods 186 (1981) 91.

25 - P. Dabkiewicz, F. Buchinger, H. Fisher, H.J. Kluge, H. Kremling, T. Kühl, A.C. Müller and H.A. Schuessler,
Phys. Lett. 82B (1979) 199.

26 - J. Bonn, G. Huber, H.J. Kluge and E.W. [illegible]en,
Z. Phys. A276 (1976) 203.

27 - C. Bourgeois et al. Int. Conf. on Nuclear Physics. LBL-Berkeley (1980)
- C. Bourgeois, M.G. Desthuilliers-Porquet, P. Kilcher, B. Roussière, J. Sauvage-Letessier and the ISOCELE Collaboration, 4th Int. Conf. on Nuclei far from Stability, HELSINGØR (1981), CERN 81-09, p.618.

28 - A. Marion and S. Equilbey,
C.D.S.I., Internal Report, ORSAY (1978).

29 - P. Paris and J. Tréherne,
Rev. Phys. Appl. 4 (1969) 291.

30 - P.G. Hansen, H.L. Nielsen, K. Wilsky, M. Alpsten, M. Finger, A. Lindahl, R.A. Naumann and O.B. Nielsen,
Nucl. Phys. A148 (1970) 249.

31 - C.M. Lederer and V.S. Shirley,
Table of Isotopes, 7th Edition (Wiley, New-York, 1978).

32 - N.B. Gove and M.J. Martin,
Nucl. Data Tables 10 (1971) 205.

33 - V. Berg, Z. Hu, J. Oms and the Isocele Collaboration,
4th Int. Conf. on Nuclei far from Stability, HELSINGØR (1981), CERN 81-09, p. 628.
- V. Berg, Z. Hu and J. Oms,
to be published.

34 - S. Raman and N.B. Gove,
Phys. Rev. C7 (1973) 1995.

35 - J.W. Grüter, B. Jonson and O.B. Nielsen,
3rd Int. Conf. on Nuclei far from Stability, CARGESE (1976),
CERN Report 76-13 (1976) 428.

36 - A. Visvanathan, E.F. Zganjar, J.L. Wood, R.W. Fink, L.L. Riedinger and F.E. Turner,
Phys. Rev. C19 (1979) 282.

37 - J. Meyer-ter-Vehn,
Nucl. Phys. A249 (1975) 111 and 141.

38 - M. Meyer, J. Danière, J. Letessier and P. Quentin,
Nucl. Phys. A316 (1979) 93.

39 - J. Libert, Thesis, Univ. of Paris VII (1981)
- M.G. Desthuilliers-Porquet, M. Meyer, P. Quentin and J. Sauvage-Letessier, 4th Int. Conf. on Nuclei far from Stability, HELSINGØR (1981), CERN 81-09, p. 623.
- J. Libert, M. Meyer, P. Quentin, Phys. Rev. C25 (1982) 586.
- J. Libert, M. Meyer, P. Quentin, Phys. Lett. 95B (1980) 175.

40 - R. Béraud, M. Meyer, M.G. Desthuilliers, C. Bourgeois, P. Kilcher and J. Letessier,
Nucl. Phys. A284 (1977) 221.

41 - A. Ben Braham et al.,
Nucl. Phys. A332 (1979) 397.

42 - E.F. Zganjar, J.D. Cole, J.L. Wood, M.A. Grimm,
4th Int. Conf. on Nuclei far from Stability, HELSINGØR (1981),
CERN 81-09, p. 630.

43 - G.M. Gowdy, Ph. D. thesis, School of Chemistry, Georgia Institute of Technology (1976).
- G.M. Gowdy, J.L. Wood and R.W. Fink,
Nucl. Phys. A312 (1978) 56.

44 - Ch. Vieu, S.E. Larsson, G. Leander, I. Ragnarsson, W. de Wieclawik and J.S. Dionisio,
Z. Phys. A290 (1979) 301.

45 - J.L. Wood,
Phys. Rev. C24 (1981) 1788.

46 - W.M. Lattimer, K.S. Krane, N.J. Stone and G. Eska,
J. Phys. G : Nucl. Phys. 7 (1981) 1713.

FIGURES CAPTIONS

Fig. 1 - Partial singles gamma-ray spectrum measured with a planar Ge(HP) detector. The gamma-ray energies are given in keV. Collection and measurement time for ^{185}Hg sources was 30 sec. (The 310.6 keV γ-ray line belongs to ^{185}Pt).

Fig. 2 - Selected coincidence spectra for $^{185m+g}$Hg decay corresponding to gates set on the 193.0, 205.2 + 205.7, 211.1, 212.5, 292.4, 349.0 keV γ-ray lines. BS refers to coincident backscattered peak.

Fig. 3 - Low-energy electron microdensitogram from a film obtained with the β-spectrograph ($B = 4.2\ 10^{-3}$ Tesla). Lines assigned to transitions in ^{185}Au are marked by their corresponding γ-ray energy and the converting electron shell. The ^{185m}Hg decay lines corresponding to transitions in ^{185}Hg are marked by Hg.

Fig. 4 - Medium-energy electron microdensitogram from a film obtained with the β-spectrograph ($B = 1.3\ 10^{-2}$ Tesla). The ^{185}Au decay lines corresponding to the 77.6 keV transition in ^{185}Pt are designated by Pt.

Fig. 5 - Decay scheme for $^{185m+g}$Hg to levels in ^{185}Au (Part I). The dashed lines were observed in singles spectra only. The arrow widths indicate total intensities. Transitions connecting different intrinsic configurations are shown slanted. For sake of clearness, the high-spin levels of the $h_{9/2}$ family are shown apart from the low-spin levels. The abnormally converted M1 transitions are marked by an asterisk.

Fig. 6 - Decay scheme for ^{185g}Hg to levels in ^{185}Au (Part II). cf. Caption to fig. 5.

Fig. 7 - The decay of ^{185m}Hg : low-energy levels in ^{185}Hg.

Fig. 8 - Comparison of the experimental excited states of ^{185}Au with the calculated levels using HF qp states coupled to ^{184}Pt ($\beta_2 = 0.27$) or ^{186}Hg ($\beta_2 = 0.28$) core (——levels from $h_{9/2}$ + $f_{5/2}$ subshells, ●●●● levels from $f_{7/2}$ + $p_{3/2}$ subshells, —●—●— levels from $h_{9/2}$ + $f_{7/2}$ + $f_{5/2}$ + $p_{3/2}$ subshells).

a) high-spin states (19/2- and 21/2- levels were taken from the ref.[11]).

b) low-spin states.

Fig. 9 - Experimental levels as rotational bands built on different HF states (HFa = sixth 3/2- HF state, HFb = eighth 1/2- HF state, HFc = fourth 5/2- HF state, HFd = ninth 1/2- HF state). Double-lines indicate experimental transitions with large total intensity ($I \geq 40$), single-lines transitions with medium intensity ($10 < I < 40$) and dashed-lines transitions with weak intensity ($I \leq 10$).

Fig. 10 _ Systematics of experimental levels and theoretical [37] states arising from the $h_{11/2}$ subshell.

Fig. 11 - Comparison of the low-lying positive-parity states of ^{185}Au with the calculated levels using HF qp-states coupled to oblate ^{186}Hg ($\beta_2 = -0.19$) or prolate ^{186}Hg ($\beta_2 = +0.28$) core. The 11/2- (oblate case) and 9/2- (prolate case) bandheads are also shown.

TABLE CAPTIONS

Table 1 - Gamma-ray and internal conversion-electron data for the decay of $^{185m+g}Hg$ to ^{185}Au (collection and measurement time for ^{185}Hg sources was 30 s).

notes : + intensity error ∿ 30% (otherwise intensity error ∿ 10%)

* the multipolarity has also been deduced from (HI,xnγ) experiments [11].

o transition mixed with a γ-ray from the decay of ^{181}Os.

Table 2 - Internal conversion-electron data for the decay of ^{185m}Hg to ^{185g}Hg. The intensities of the electron lines are determined per 100 decays of ^{185m}Hg.

Table 3 - Weight of the main components of the low-energy negative parity state wave-functions in terms of the |nljR> basis.

TABLE 1

E_γ (keV)	Main feeding	I_γ	I_e	α_{exp}	Multipolarity	I_{tot}	Main coincident γ-rays
17.17 ± 0.03			M_I 30<I_e<74		M1+(1.6 ± 1.4)% E2	525 ± 175	
			M_{II} 17				
			M_{III} 18				
23.6 ± 0.1			L_I 460		M2	900	
			L_{II} 23				
			L_{III} 260				
			M_I 110				
			M_{II} 13				
			M_{III} 78				
35.75 ± 0.05			L_I 100		M1+ 20% E2	770	(129.1), 222.9, 244.2
			L_{II} 230				
			L_{III} 250				
			M_I 18				
			M_{II} 50				
			M_{III} 70				
97.4 ± 0.1		1.6+					
98.5 ± 0.1		8.4+	K 56	6.7	M1	72	181.0, 193.7, 205.2, 222.9. 558.9
107.4 ± 0.1		4+	K 9	2	M1 + 60% E2	17	181.0, (193.7), (222.9)
107.8 ± 0.1		6+	K 23	4.5	M1 + 25% E2	31	244.2
119.1 ± 0.2		0.7+	K ∿2	∿3	(M1 + E2)	∿4	
124.1 ± 0.2	} g	3+	K 6.5	2.2	M1 + 30% E2	11	178.5, 193.0, 325.2,(330.2)
125.1 ± 0.2		2.4+	K 5.3	2.2	M1 + 30% E2	9	
			L_I < 3				
129.1 ± 0.1	g	13.1	K 26	2	M1 + 30% E2	45	222.9, 258.7,(431.9), 898.2
			L_I 4.5				
			L_{II} <0.7				
			L_{III} <0.7				
130.6 ± 0.2		0.7+	K 2.6	3.5	M1	3	
146.4 ± 0.2		2+	K 4.3	2.2	M1	7	
152.8 ± 0.2		3+	K 3	1	M1 (+ 50% E2)	9	(178.5), 250.3
			L_I+L_{II} 2				
164.9 ± 0.2		2.4+	K mixed				(250.3)
165.8 ± 0.2		2.7+	K mixed				250.3, (401.8), 459.5
178.5 ± 0.1		4.5	K mixed				124.1,(152.8),(193.0), 250.3 325.2, (391.8)
180.5 ± 0.2			K		E2*		558.9
181.0 ± 0.1	g	8.6	K < 9	<1		<18	98.5, 107.4, 283.4
190.1 ± 0.1	g	49	K 40	0.85	M1 (+E2)	97	239.6, 244.1,(371.6), 403.4, 600.0
			L_I+L_{II} mix.				
			M_I+M_{II}+M_{III} 2.2				
193.0 ± 0.1	} m + g	42	K 24	0.58	M1 + 50% E2	73	(124.1), 178.5, 205.7, 325.2, 349.0, 366.9, (480.0)
			L_I+L_{II} 3.5				
			L_{III} 0.6				
193.7 ± 0.1		13.5	K 2	0.15	E2	18	98.5, 107.4, 315.3, 558.9
			L_I+L_{II} 0.6				

E_γ (keV)	Main feeding	I_γ	I_e		α_{exp}	Multipolarity	I_{tot}	Main coincident γ-rays
205.2 ± 0.2		8.4	K	11	1.3	E0+M1 (+E2), abn M1	22	98.5, 222.9, 321.4, 330.2,
			L_I+L_{II}	1.6				416.2, (614.5).
205.7 ± 0.2		6.4	K	1.3	0.18	(E2)	8	193.0, 350.2
210.4 ± 0.1		12.4	K	~2	~0.17	(E2)	16	205.7, 325.2, 349.0, 366.9
211.2 ± 0.1	m	47	K	30	0.63	M1	85	270.1,(376.5), 461.0, 462.2,
			L_I+L_{II}	8				491.9, 550.8, (582.2).
212.5 ± 0.1	m	55	K	9	0.16	E2	66	243.6, 265.7,(315.3), 322.7
			L_I+L_{II}	~6				395.2, 424.1, 426.7, 555.2,
								558.9, 639.2,(776.1).
222.8 ± 0.1	g	100	K	51	0.51	M1 + 25% E2	164	129.1, 205.2, 313.2,(451.9)
			L_I	7.7				(580.5), 614.3, 674.7,
			L_{II}	?				777.9, 1027.2
			L_{III}	1.4				
239.6 ± 0.2	g	8.4	K	5	0.6	M1	15	190.1
			ΣL	~4				
243.1 ± 0.2		~9	K	~2.5	~0.3	M1 + E2	~15	190.1, 403.4.
243.6 ± 0.2		~4						212.5, 292.2, 315.3.
244.2 ± 0.1		42	K	20	0.47	M1	66	107.8, 451.9,(653.6), 756.7
								898.2, 1014.4.
250.3 ± 0.2	g	37	K	17	0.47	M1	58	(164.9), 165.8, 391.8.
			ΣL	2.5				
252.7 ± 0.1		7	K	2.6	0.38	M1 + 25% E2	10	283.4
			ΣL	0.8				
258.7 ± 0.1	g	92	K	40	0.43	M1	140	129.1,(276.6), 313.2, 451.9
								580.5,(674.7),(777.9),
								(898.2),(1027.2).
267.6 ± 0.2		5.4	K	~1.3	~0.24	M1 + E2	~7	
270.1	g	9.8	K	0.6	0.06	E1, E2	~11	211.2,(376.5), 582.2,(746.7)
276.6		2.7	K	~1	~0.4	M1	~4	(222.9),(258.7).
280.1		9	K	~0.7	~0.07	(E2)	~10	
283.4	g	8.2	K	2.4	0.3	M1 (+E2)	11	181.0, 288.7,(252.7).
288.7	g	19.8	K	~8	~0.4	(M1)	~28	283.4
292.4	m	34.2	K	5.2	0.15	M1 + 70% E2	42	243.6, 315.3, 369.0, 424.1,
								558.9,(564.2).
302.9		3.3						(205.2),(222.8), 325.2
309.0		2.2						(292.2).
313.2		10	K	~4.5	~0.45	E0+M1(+E2),abn.M1	~16	222.9, 258.7.
315.3	m	9.7	K	0.6	0.06	E2*	10	98.5, 193.7, 243.6, 292.4,
								424.1.
321.4	m+g	7	K	3.3	0.47	E0+M1(+E2),abn.M1	11	205.2.
322.7		10.2	K	0.4	0.04	E2*	11	212.5.
325.2	m	10.9	K	2.9	0.27	M1	14	124.1, 152.8, 193.0, 210.4,
								331.7,(389.5).
330.2	g	14.2	K	16	1.1	E0+M1(+E2),abn.M1	33	205.2.
			ΣL	2.3				
331.7		~2.1	K	0.1	~0.05		~2.5	(193.0),(325.2).
336.7	g	30	K	6	0.21	M1	37	(205.2),(250.3),(725.8).
340.2		2.5	K	~0.05	~0.02	E1	~2.5	
345.2		0.5	K	< 0.05	< 0.1		~0.6	190.1,(124.1).
347.5	g	12.2	K	3	0.21	M1	16	461.0.
349.0		17.6	K	1	0.054	E2	19	193.0, 210.4, 366.9.
350.2		4.8	K	~0.3	~0.06	(E2)	5	205.7, 377.5, 398.7.
361.6		3.3						

E_γ (keV)	Main feeding	I_γ	I_e	α_{exp}	Multipolarity	I_{tot}	Main coincident γ-rays
365.1		1.6					
366.9	m	8.8	K < 0.27	<0.03	E1, E2	9	193.0, 210.4, 349.0.
369.0		1.8					558.9.
371.6		3.0					190.1, 480.0.
376.5		1.6					
377.5		3.3					(193.0),(210.4), 350.2, (398.7).
382.9		1.6					
384.8		2.0					
388.3		2.8					
389.5		2.2					325.2
391.8		2.7					(152.8), 178.5, 250.3,(331.7)
395.2		4.1	K ∿ 0.16	∿ 0.04	E2, M1 + E2	4.5	212.5, 424.1.
398.7		13.3	K ∿ 0.4	∿ 0.03	(E2)	14	350.2,(376.5),(421.8).
401.8		3.5					
403.4		3.1					190.1, (243.1).
412.6		1.7					
414.8		1.7					
416.2		10.5	K mixed				
417.9		3.0					
421.8		1.8					193.0, 205.7, 398.7.
424.1		3.5					212.5, 292.4, 315.3, 395.2
426.6		1.8					212.5.
429.8		10.0	K ∿ 0.4	∿ 0.04	E2 + M1	10.5	
433.2		3.7					
438.0 ± 0.3		2.3					292.2, 558.9.
449.0 ± 0.2		2.1					(178.5),(212.5).
451.9		5.6	K ∿ 0.6	∿ 0.11	M1	6.5	107.8, 129.1, 222.9, 244.2, 258.7.
455.5		1.6					
459.5		1.6					
461.0	} m	17.1	K 0.7	0.04	M1 + E2	18	211.2, 347.5.
462.2		8.7	K 0.2	0.02	E2	9	211.2
464.3		3.1					
473.6		8.4					
480.0	m + g	13.2					371.6
491.9		3.8					211.2
524.6		1.4					
527.1		1.5					
536.1		11.7					
542.3		0.8					
545.2		5.4					(222.9),(244.2),(258.7).
550.8		6.8					
555.2		5.9					212.5, (713.2).
558.9		16.2					19..7, 292.2,(369.0), 438.0.
561.1		1.5					(193.0), 205.7
564.3		1.1					
572.2		3.0					
576.9		2.0					
578.8		2.7					
580.5		5.6					222.9, 258.7.
582.2		5.2					211.2, 270.1.
584.6		1.4					
593.5		11.4					

E_γ (keV)	Main feeding	I_γ	I_e	α_{exp}	Multipolarity	I_{tot}	Main coincident γ-rays
600.0		3.6					190.1
604.6		1.6					
605.7		3.6					
612.8		3.0					
614.3		4.7					222.9, 258.7
622.5		4.0					
631.0		2.0					
639.2		3.1					212.5
653.6		1.1					
674.7		4.3					(222.9), (258.7).
682.5		1.0					
746.7		2.1					
750.0		2.3					
756.7		2.4					
770.0		5.4					
772.9		2.2					
776.1		2.0					
777.9		6.2					222.9, 258.7.
790.6		2.4					
804.5		5.7					
808.4		1.2					
821.1		0.5					
827.3[o]		1.6					
831.3[o]		7.4					
836.3		6.4					
840.2		8.7					
867.9		4.9					
871.6		2.2					
875.5		3.4					
898.2		5.9					129.1, 222.9, 244.2, 258.7.
918.9		3.9					
957.3		2.0					
992.4		7.5					
997.1		2.9					
1000.8		1.8					
1007.2		2.0					
1014.4		2.2					
1027.2		4.2					(222.9), 258.7.
1036.6		3.1					
1055.6		2.4					
1114.5		2.0					
1164.7		2.5					
1250.2		2.2					
1258.6		2.5					
1286.1		3.4					

TABLE 2

E_γ (keV)	I_e		Multipolarity	I_{tot}
26.1	L_I	: $16 < I_e < 18.8$	M1 + E2	71 ± 22
	L_{II}	: $12.3 < I_e < 20.9$	($0.5\% < \delta^2 < 3.5\%$)	
	L_{III}	: $8.6 < I_e < 22.1$		
	M_I	: 5.5		
	M_{II}	: 4.4		
	M_{III}	: 5.4		
65.3	L_I	: $I_e < 0.7$	E3	54 ± 10
	L_{II}	: 14.2		
	L_{III}	: 12.3		
	$M_I + M_{II}$	: 3.7		
	M_{III}	: 3.3		
	$M_{IV} + M_V$	: 0.9		

TABLE 3

I	E_{exp} keV	E_{th} keV	R	nlj									
				1p3/2	2p3/2	4p3/2	1f5/2	3f5/2	1f7/2	3f7/2	1h9/2	2h9/2	1h11/2
$5/2^-$	0	0	0				10%						
			2								30%	19%	
			6								11%	7%	
$9/2^-$	8.9	63	0								21%	13%	
			2				13%	6%			14%	9%	
			8								5%		
$3/2^-$	17.2	23	2				14%	6%					
			4								35%	23%	
$7/2^-$	107.4	105	2				7%				12%	8%	
			4				6%				18%	11%	
			6								5%		
$3/2^-$	190.1	142	0		10%	6%							
			2		10%	6%			9%	11%			
			4							5%			6%
$1/2^-$	210.4	516	2				20%	10%					
			4								38%	26%	
$13/2^-$	221.4	267	2								31%	19%	
			4				14%	6%			7%	5%	
$1/2^-$	267.5	233	2	8%	20%	12%							
			4						13%	15%			
			6										9%
$7/2^-$	288.7	235	0							5%			
			2	5%	13%	8%			5%	5%			
			4		6%								

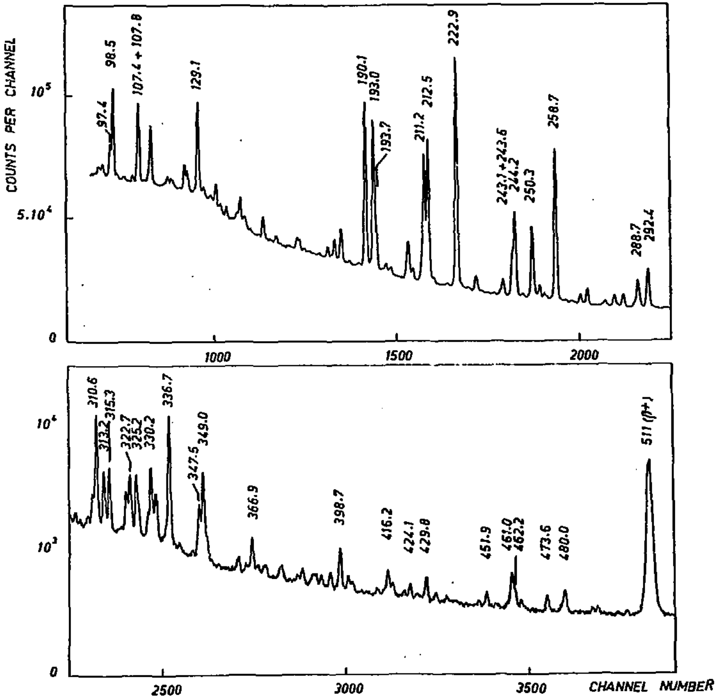
COUNTS PER CHANNEL
10^5
5.10^4
0
97.4
98.5
107.4 + 107.8
129.1
190.1
193.0
193.7
211.2
212.5
222.9
243.1 + 243.6
244.2
250.3
258.7
288.7
292.4
1000
1500
2000
10^4
10^3
0
310.6
313.2
315.3
322.7
325.2
330.2
336.7
347.5
349.0
366.9
398.7
416.2
424.1
429.8
451.9
461.0
462.2
473.6
480.0
511 (β+)
2500
3000
3500
CHANNEL NUMBER

fig 1

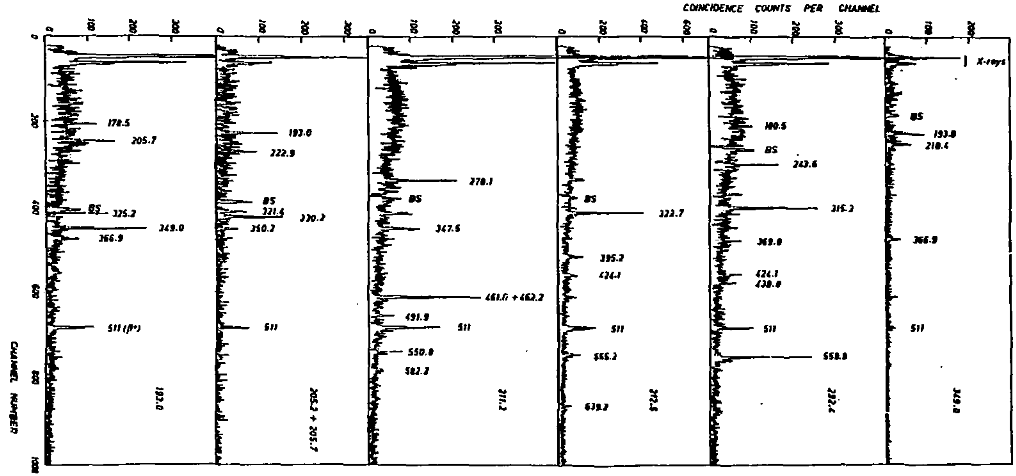

COINCIDENCE COUNTS PER CHANNEL
CHANNEL NUMBER
X-rays
178.5
205.7
BS
325.2
349.0
366.9
511 (β+)
193.0
193.0
222.9
BS
321.4
330.2
350.2
511
205.3 + 205.7
278.1
BS
347.6
461.6 + 462.2
491.9
511
550.8
582.2
311.2
BS
323.7
395.2
424.1
511
556.2
639.2
312.5
180.5
BS
243.6
315.2
369.0
424.1
438.0
511
558.8
332.6
BS
193.8
210.4
366.9
511
349.0

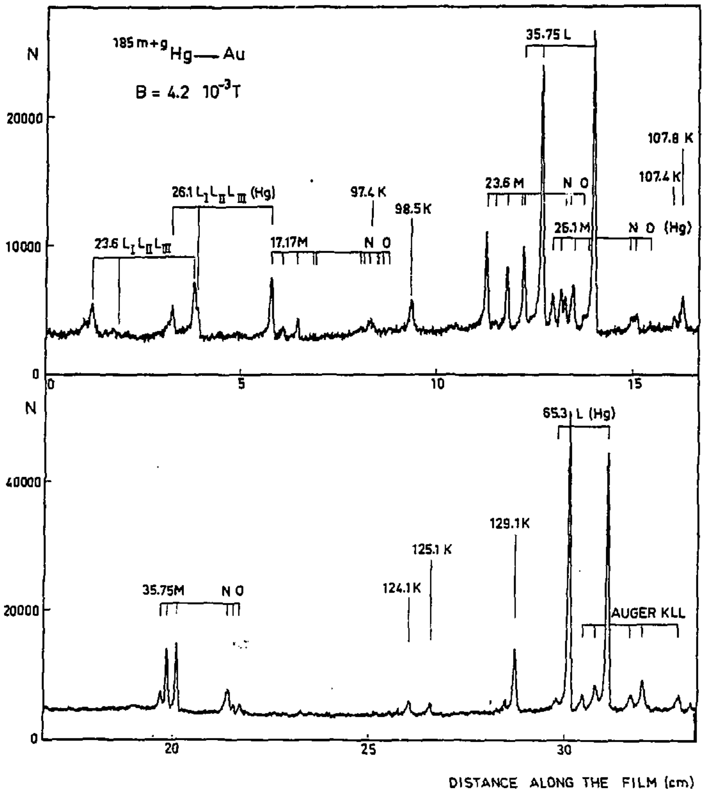

N
185m+g Hg — Au
B = 4.2 10^-3 T
20000
10000
0
35.75 L
107.8 K
107.4 K
23.6 M
N O
26.1 M
N O (Hg)
26.1 L_I L_II L_III (Hg)
97.4 K
98.5 K
23.6 L_I L_II L_III
17.17M
N O
0
5
10
15
N
65.3 L (Hg)
40000
20000
0
129.1K
125.1 K
124.1 K
35.75M
N O
AUGER KLL
20
25
30
DISTANCE ALONG THE FILM (cm)

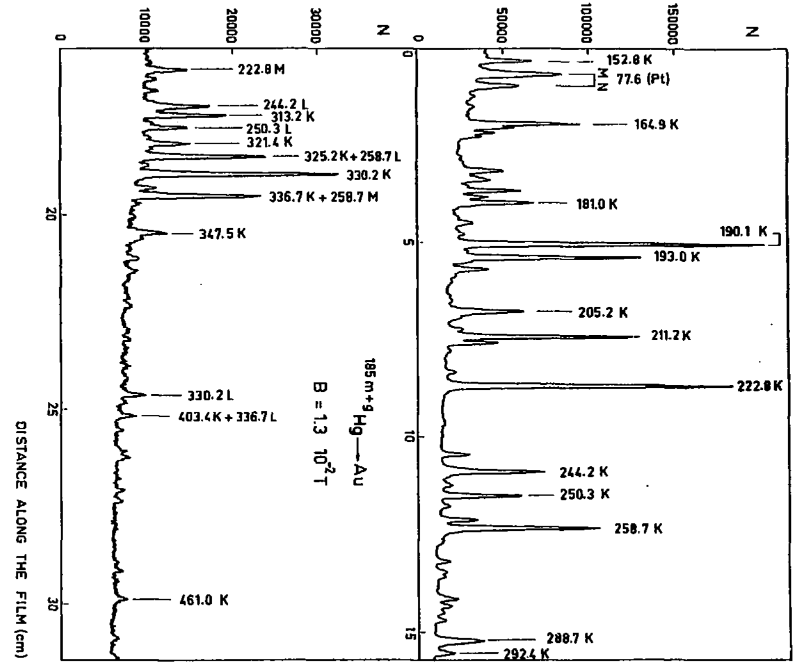

$^{185m+g}$Hg—Au
B = 1.3 10^{-2} T
N
DISTANCE ALONG THE FILM (cm)
152.8 K
77.6 (Pt)
M
N
164.9 K
181.0 K
190.1 K
193.0 K
205.2 K
211.2 K
222.8 K
244.2 K
250.3 K
258.7 K
288.7 K
292.4 K
222.8 M
244.2 L
313.2 K
250.3 L
321.4 K
325.2 K + 258.7 L
330.2 K
336.7 K + 258.7 M
347.5 K
330.2 L
403.4 K + 336.7 L
461.0 K

Part I

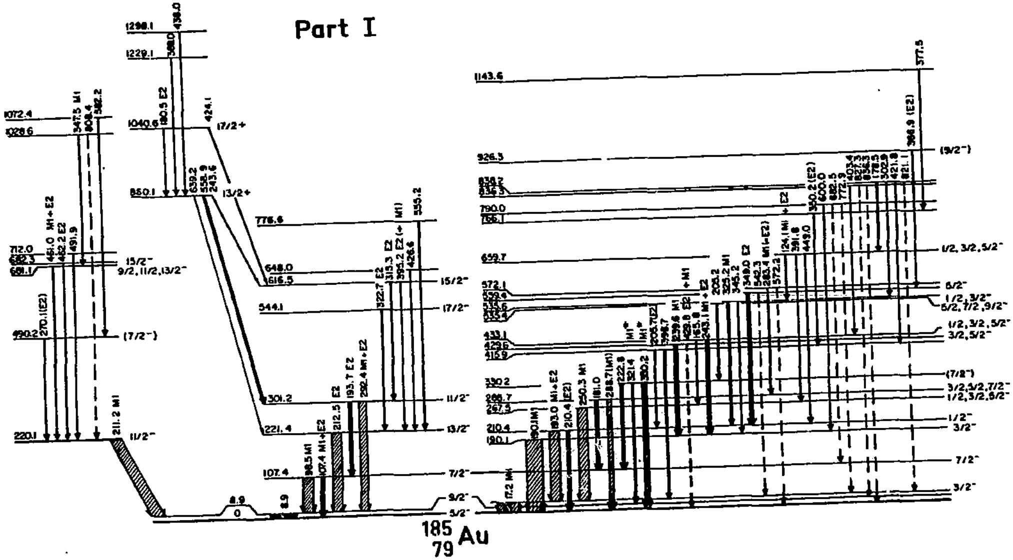

Part II

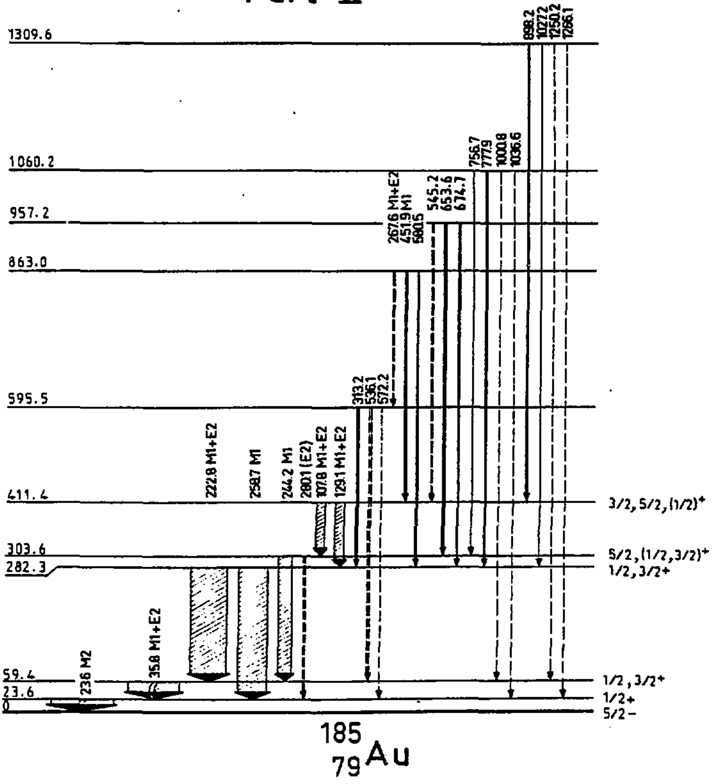

1309.6
1060.2
957.2
863.0
595.5
411.4
303.6
282.3
59.4
23.6
0
898.2
1027.2
1250.2
1286.1
756.7
777.9
1000.8
1036.6
267.6 M1+E2
451.9 M1
580.5
545.2
653.6
674.7
313.2
536.1
572.2
222.8 M1+E2
258.7 M1
244.2 M1
280.1 (E2)
107.8 M1+E2
129.1 M1+E2
35.8 M1+E2
23.6 M2
3/2, 5/2, (1/2)+
5/2, (1/2, 3/2)+
1/2, 3/2+
1/2, 3/2+
1/2+
5/2−
185
79 Au

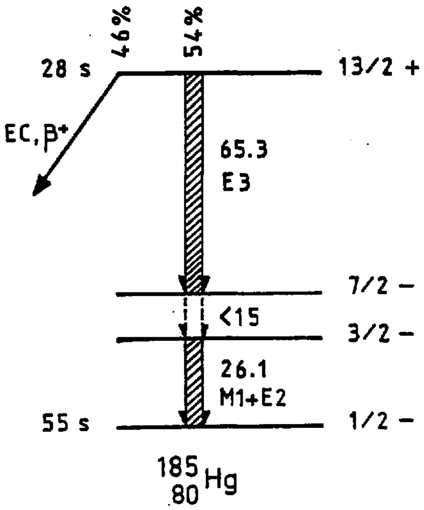
46%
54%
28 s
13/2 +
EC, β+
65.3
E3
7/2 −
<15
3/2 −
26.1
M1+E2
55 s
1/2 −
185
80
Hg

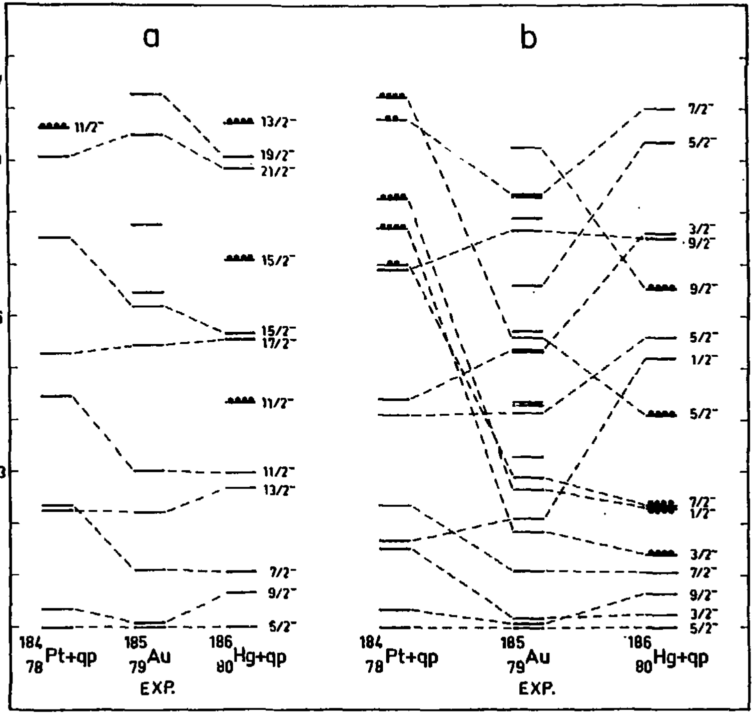

a
b
E
MeV
0.9
0.6
0.3
0
11/2⁻
13/2⁻
19/2⁻
21/2⁻
15/2⁻
15/2⁻
17/2⁻
11/2⁻
11/2⁻
13/2⁻
7/2⁻
9/2⁻
5/2⁻
7/2⁻
5/2⁻
3/2⁻
9/2⁻
9/2⁻
5/2⁻
1/2⁻
5/2⁻
7/2⁻
1/2⁻
3/2⁻
7/2⁻
9/2⁻
3/2⁻
5/2⁻
$^{184}_{78}$Pt+qp
$^{185}_{79}$Au
EXP.
$^{186}_{80}$Hg+qp
$^{184}_{78}$Pt+qp
$^{185}_{79}$Au
EXP.
$^{186}_{80}$Hg+qp

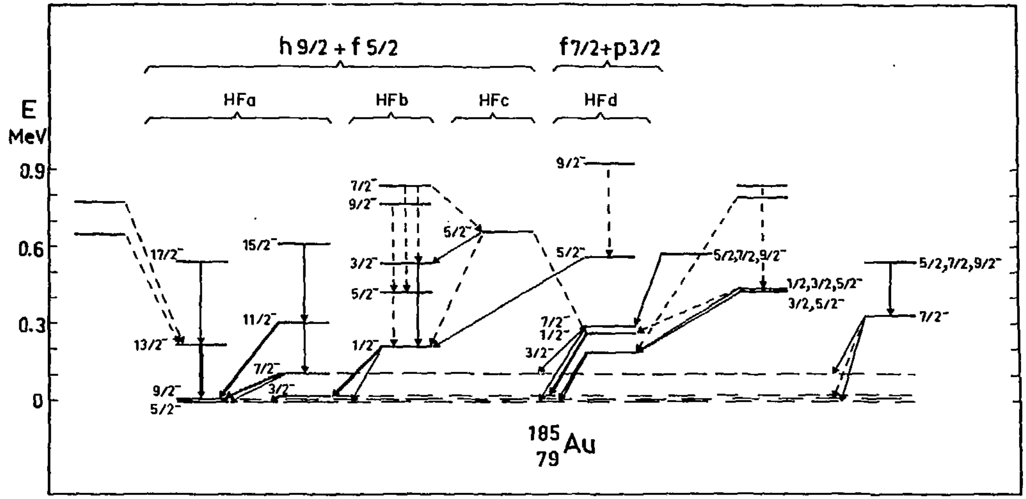

h 9/2 + f 5/2
f7/2+p3/2
HFa
HFb
HFc
HFd
E
MeV
0.9
0.6
0.3
0
17/2⁻
13/2⁻
9/2⁻
5/2⁻
15/2⁻
11/2⁻
7/2⁻
3/2⁻
7/2⁻
9/2⁻
3/2⁻
5/2⁻
1/2⁻
5/2⁻
9/2⁻
5/2⁻
7/2⁻
1/2⁻
3/2⁻
5/2,7/2,9/2⁻
1/2,3/2,5/2⁻
3/2,5/2⁻
5/2,7/2,9/2⁻
7/2⁻
185
79 Au

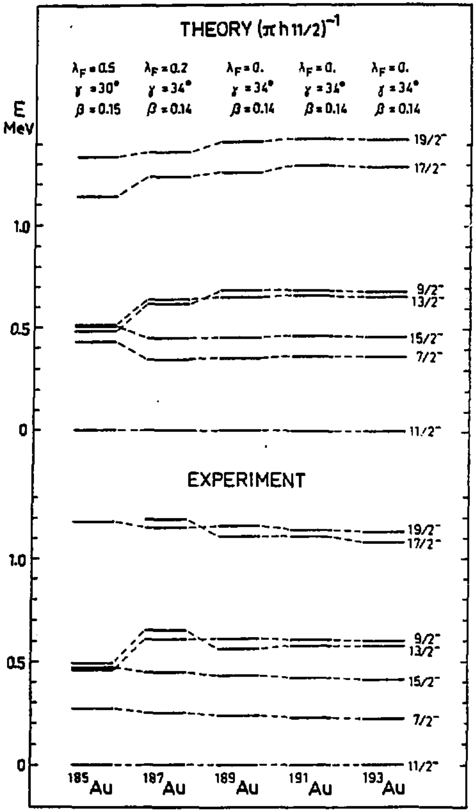
THEORY (π h 11/2)^-1
λF = 0.5 γ = 30° β = 0.15
λF = 0.2 γ = 34° β = 0.14
λF = 0. γ = 34° β = 0.14
λF = 0. γ = 34° β = 0.14
λF = 0. γ = 34° β = 0.14
E MeV
1.0
0.5
0
19/2⁻
17/2⁻
9/2⁻
13/2⁻
15/2⁻
7/2⁻
11/2⁻
EXPERIMENT
185Au
187Au
189Au
191Au
193Au

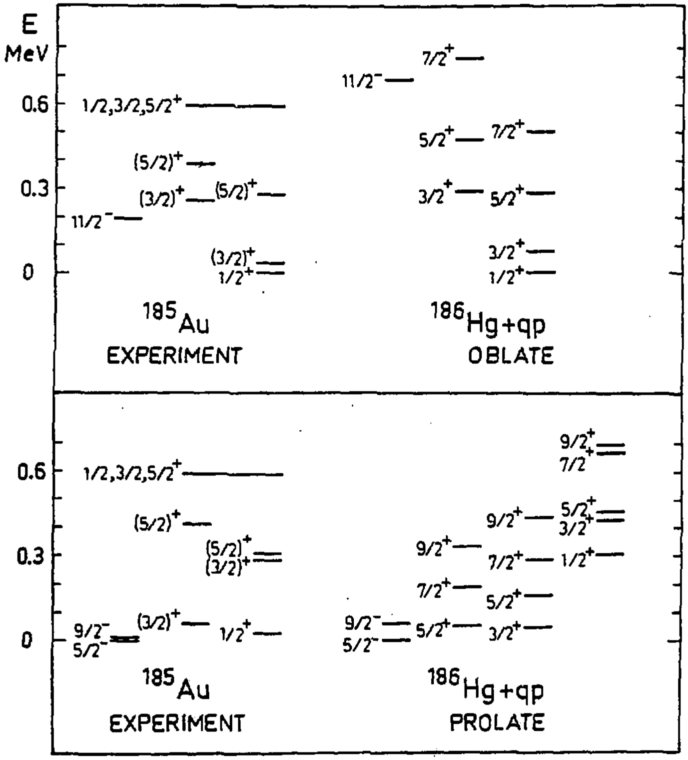
E
MeV
0.6
0.3
0
1/2,3/2,5/2+
(5/2)+
(3/2)+
(5/2)+
11/2−
(3/2)+
1/2+
7/2+
11/2−
5/2+
7/2+
3/2+
5/2+
3/2+
1/2+
185Au
EXPERIMENT
186Hg+qp
OBLATE
0.6
0.3
0
1/2,3/2,5/2+
(5/2)+
(5/2)+
(3/2)+
9/2−
5/2−
(3/2)+
1/2+
9/2+
7/2
9/2+
5/2+
3/2
9/2+
7/2+
1/2+
7/2+
5/2+
9/2−
5/2−
5/2+
3/2+
185Au
EXPERIMENT
186Hg+qp
PROLATE